ORIGINALLY PUBLISHED & PRESENTED AT ECTC 2019

SB²-WB: A new process solution for advanced wire-bonding

Matthias Fettke, Andrej Kolbasow, Georg Friedrich, Anna Palys, Vinith Bejugam and Thorsten Teutsch
PacTech GmbH
Am Schlangenhorst 7-9, 14641 Nauen, Germany
Phone: +49 (0)3321 4495-504, Fax: +49 (0)33214495-110, E-Mail: fettke@pactech.de

***Abstract*—This paper describes a novel and innovative wire-bonding method which combines standard wire feeding application with the unique solder-jetting process; i.e. SB²-Jet. In contrast to conventional ultrasonic, thermosonic or thermocompression bonding, the laser-wire-bond connection, SB²-WB, is not welded but soldered. Neither pressure, ultrasonic vibration nor high temperatures are utilized. These technical advancements broaden the spectrum of wire-bonding applications. Besides the fundamental process explanation and the comparison to conventional wire-bonding methods, the results of initial reliability and stability tests on 50µm Au wire contacts bonded in wedge-wedge configuration are presented and discussed. For this comparison, the bonds were thermally, mechanically and electrically stressed. The impact on the bonds after thermal cycling (250TW) and vibration tests were microscopically inspected and metallurgically studied through cross-sectional polishing and FIB-SEM characterization. The mechanical load-capacity was quantified using a pull and shear test measurement system. The failure characteristics of the bonds during an ampacity test were analyzed by thermal imaging.**

Moreover, the fabrication of laser-wire-bond connections on a piezoceramic element as part of a PDC-ultrasonic sensor using 80µm insulated Cu wire and SAC_305 (760µm sphere diameter) solder alloy is described and qualified as an example of potential application. The mechanical strengths of the interconnections were measured using a shear tester, while the concomitant metallurgical properties were analyzed by X-ray and FIB-SEM. The opportunity to remove surrounding insulation material of a wire during the bonding process will be an additional topic of discussion.

Finally, a roadmap for this new technology and future prospects involving intended reliability and comparative stability studies are elucidated.

***Keywords:* wire-bonding, wire-soldering, solder-jetting, heavy wire, Cu wire, dismantling, chip packaging**

I. Introduction

In the field of semiconductor packaging, wire-bonding is the most common bonding technology for creating electrical interconnects. More than three-quarters of all IC-elements in 2018 contained primary wire-bond interconnections, which indicates the dominant and growing interest in wire-bonding technologies [1].

However, the continuous growth of the global market for micro-electromechanical components and systems entails further miniaturization and augmented performance capabilities, requiring new technologies where the standard wire-bonding processes reach an impasse. Alternative process ideas are in great demand for the partial substitution of conventional wire-bond processes on the one hand and for broadening of application fields on the other hand [2].

The common goal is to facilitate the growth of new geometrical & physical bonding capabilities as well as to increase the available material selections and material combinations.

II. Process Explanation & Description

A. General process setting

The key components of the process setting are PacTech´s unique solder-jetting unit involving, a wire feeder and a 3D axis system. In Figure. 1, the principle configuration is illustrated.

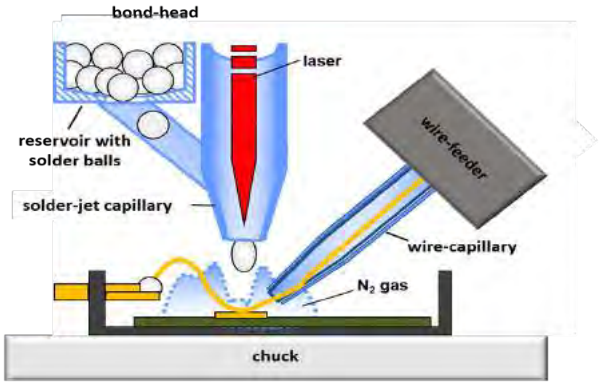

Figure 1: Process setting of laser-wire-bonding core unit

The bond-head singulates solder sphere preforms whose sizes are in the range of 30µm-1200µm, and transfers each solder sphere into a ceramic capillary. Inside the capillary, a NIR-laser induces thermal energy and liquifies the solder sphere. The liquid droplet is then expelled out of the capillary by supporting N2-pressure [3].

The wire feeder system positions the bond wire in the target area of the solder-jetting capillary. During the feeding and motion of the system, the wire is guided through a wire capillary, which is located in close proximity to the solder-bond capillary. The wire can be pushed, pulled, unwound or fixated to enable precise positioning and diverse loop designs.

The bond-table moves in x and y directions and positions the substrates with respect to the target area of the solder-jetting unit. All bonding components are mounted on the z-axis unit, which moves to the required bond-height. Distance and angle adjustments of the feeder capillary are performed manually.

In Figure 2, the developed system arrangement and configuration of the work-area for a solder-wire-bond is shown.

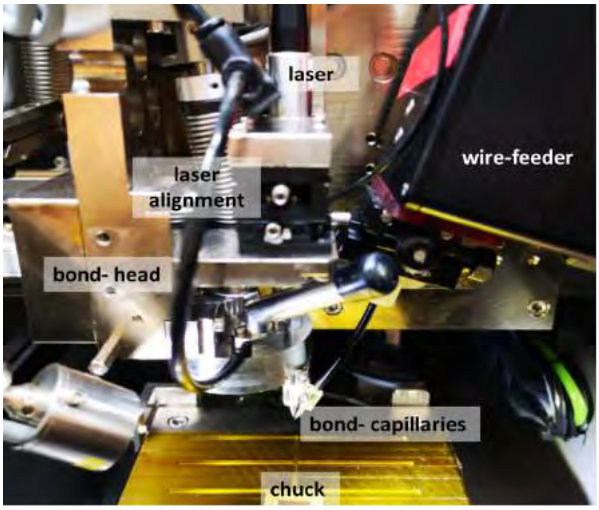

Figure 2: SB²-WB machine setup

B. General process flow

After moving the laser-wire-bonding unit to the target position of a contact pad, the wire is fed with a defined length. Depending on the adjusted position of the wire capillary, the wire is either pushed onto the pad or held in a floating condition above the pad. Parallelly, a solder droplet is prepared and applied. The liquid solder droplet bonds the wire onto the pad and creates a uniform wire-bump contact. The continuous supply of N_2 to this interface protects the involved materials against oxidation. Both process steps are performed almost synchronously. After contacting the first position, the axis-system moves to the subsequent bond location. During the movement, the wire unwinds and can be plastically manipulated to form different loop designs. Figure 3 presents multiple wire loop forms generated by the wire-bond system.

At the second position, apart from feeding, the same previous process steps are repeated and the wire is cut. To separate the wire, a cutting-blade is used. The in-built laser or a sharp edge of the capillary are alternative available options for the separation process.

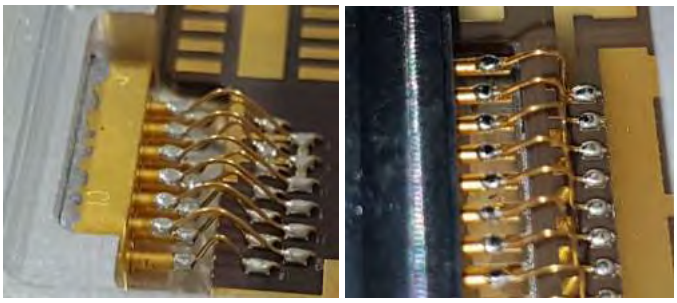

Figure 3: Laser-wire-bond (200µm Au-coated Cu wire) results on a LTCC-connector device. Left image shows a "Gaussian shape" while right image shows an asymmetric rectangular shape

C. Relevant process parameters

The solder-wire-bond quality is primarily controlled by five adjustable key-parameters: a) laser-power, b) laser-pulse-width, c) nitrogen-pressure, d) bond-distance and e) wire position. Depending upon the interaction time, kinetic force, position and thermal-intensity, the bond-shape, surface-quality, the solder coverage-level on wire and pad, specific electrical resistance, tensile strength and the ensuing characteristics of IMC-layer are affected.

The variation of the parameters in combination with different proportions of wire diameter and solder volume allows diverse geometrical bond-contact formations. As shown in Figure 4, either the wire is floating and encapsulated by the solder bump (left) or the wire is positioned on the contact-pad and bonded in the form of a volcano-shape (right).

Figure 4: Examples of possible solder-wire-bond formations

D. Temporal & thermal qualification

The temporal and thermal analysis of the laser-wire-bonding process was conducted using a fast "Optris CTvideo" pyrometer. The measurement device contains of a pyroelectric-sensor type "3MH1-CF" with a time resolution of 2ms, spectral sensitivity of 1µm, temperature resolution of 0.1K and a measurement range of 150°C-1000°C. An emissivity (ε) of 0.25 (Sn) was selected [4]. A representative measurement result of a process cycle involving 760µm SAC_305 solder ball on a 80µm Cu wire connected to a Ag-plated ceramic substrate is illustrated in Figure 5.

In order to form a homogenous, stable and reliable material interconnection between the described solder, wire and substrate configuration, a minimum NIR laser-pulse energy of 1400mJ (140W/10ms) is required.

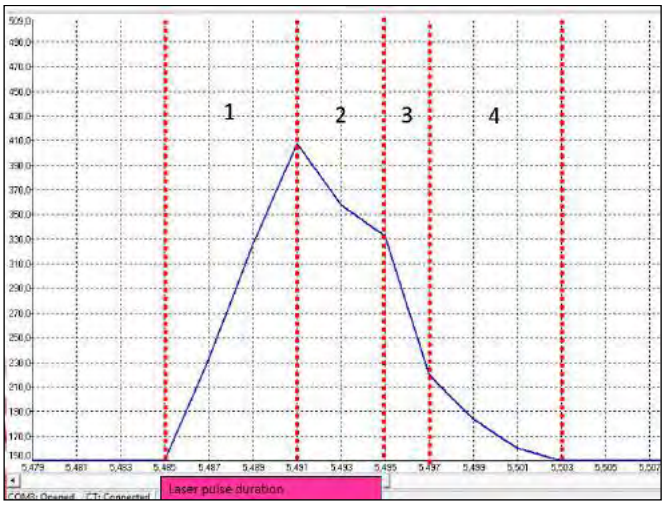

Figure 5: Temporal and thermal cycle of a SB²-WB bond (760µm, SAC_305 solder ball on 80µm Cu wire placed on an Ag-plated ceramic substrate)

Section 1 (transformation) of Figure 5 shows the thermal ramp-up of the capillary tip. Within 6ms the solder-jet capillary reaches its peak temperature of 410°C before the solder ball leaves the capillary.

Section 2 (flight-phase) represents the decreasing gradient (25K/ms) of the liquid solder ball temperature while dropping. During the flight-time, the droplet is continuously pumped with laser-energy for additional 4ms before laser switched off.

Section 3 (recrystallization) shows the cooling and interdiffusion phases of the solder ball after hitting on the substrate surface and solidifying.

Section 4 (attenuation) illustrates the typical polynomic thermal fading of the substrate-system.

E. A comparison with common wire-bond technologies

The presented curve of the thermal progression in Figure 5 shows extreme dynamic characteristics of the SB²-WB bonding process which is temporally similar to high-speed thermosonic bonding transducer times in the range of 8 to 12ms [5].

A simplified comparison between the key-characteristics of bonding processes for wires ≤ 50µm is shown in Table 1. The contents of this putative Table [2] are supplemented with new information including SB²-WB process data.

	Wire-Bond Technologies		
Parameter	**TS**	**US**	**SB²-WB**
ultrasonic power	yes	yes	no
bonding force	low (30-90cN)	low (25-45cN)	negligible (< 2µN)
temperature substrate	middle (100°C-220°C)	low (room temperature)	low (room temperature)
bonding time	short (30-100ms)	short (50-100ms)	ultra short (1-10ms)
preferred wire metal	Au, Ag, Cu, Pt, Pd	Al, Au, Cu	Au, Cu, Ag, Pd, Pt
preferred pad material	Al, Au, Cu	Al, Au, Cu	NiAu, Au, Cu
contamination	middle	middle	middle
speed	4-10 wire-bonds/s	2-3 wire-bond/s	3-4 wire-bonds/s*
min. pitch	35µm (15µm wire)	35µm (15µm wire)	40µm (15µm wire)*
	* possible but not shown		

Table 1: Comparison of bonding-parameter [2,6,7,8]

In contrast to the conventional bonding techniques, the bond substrate is not stressed by a mechanical load from the tool due to its contactless nature. Brittle materials such as LTCC, organic thin films <20µm used in MCM-D-type modules, or resonating cantilever leads which are used in optoelectronic packages can be bonded with the new technique without any impediments [8,9,10].

The structure of the wire material dictates the concomitant mechanical and electrical properties. Manipulation or transformation of the initial bulk grain structure most often is detrimental to the performance characteristics of the wire. Conventional bonding processes changes the material structure locally either by forming the ball with EFO or by ultrasonic vibration during the deformation sequence on the interface. Diagnosis of this effect is possible by analysing the fracture-modes of mechanical stress tests where the wire breakage frequently occurs along the HAZ as "neck-break". An additional and frequent consequence of wire weakening during EFO ball generation is the forming of higher loop heights [11]. By soldering the wire using the method introduced herein, neither the diameter of the wire is altered nor bulk properties are affected by recrystallization processes. This method is advantageous especially for a continuous wire-bond connection of multiple landing platforms. The thermal load for the interface is extremely low and provides significant metallurgical advantages compared to other solder reflow processes due to the generation of only few microns thick acicular IMC-layer [12,13]. The mechanisms of various loop formations during cold deformation in the material are identical for common technologies as well as SB²-WB.

Aluminium still is a dominating material for wire-bond applications pertaining to mono- or multi-metallic and ribbon or thick wires-bonds. Stable and reliable welding results confirm the capability of the conventional wire-bonding processes to inter-diffuse the already existing ~5nm oxidized surface layers [14]. For packages requiring Al as the bond material, the wire-soldering process is not applicable.

Normal or folded ULL´s as well as SSB loop formations enable minimum loop heights of <80µm. The bonding sequences takes longer and affects the productivity. The wire feeder position of a SB²-WB setting can be manipulated in a hemispherical workspace thus realizing wire-bond processes in the working range of 0°-90°. Consequently, wire-bond connections with a height corresponding to the used wire thickness is feasible [15].

Compared with a mono-metallic welded interconnection a soldered one is basically less stable and less reliable. Additionally, due to the melting temperatures of the used soft solder alloys (< 350°C), the wire-bond soldering process is not applicable for high temperature applications.

III. JOINT RELIABILITY

For the initial mechanical and electrical performance characterization of the developed wire-bond technique, TS and SB²-WB bonded wire samples were subjected to reliability tests and qualified. Common test material for both the processes was a 1mm² area and 140µm thick Si-chip with simple contact structure and 5µm ENEPIG pad plating [16,8]. The chip was mounted on a 4mm² area and 400µm thick "Kovar"-substrate with a 50µm Au plating. A 50µm Au wire (Heraeus BW AU HD2 WR) was bonded in a ball-wedge configuration to function as the connection between the 200µm

octagonal pads on the chip and the "Kovar"-substrate surface. The TS bonds were formed on a "F&S-Bondtec series 58" system and qualified based on tests pertaining to mechanical, thermal and electrical stress (Figure 6). The metrology used in these tests included a pull and shear tester ("XYZTEC Condor Sigma" & "Dage BT 4000").

Figure 6: Test chip configuration with Au-wire-bonds on "F&S Bondtec system". Left image shows the bond situation. Right image shows the TS-bonds.

The SB²-WB-bonds were generated on a "PacTech SB²-WB" prototype system (Figure 7). For sufficient coverage, a 200µm SAC_305 solder sphere was used. Loop height and bond-length were adjusted to mimic TS-bond parameters and loop forms. The wire was soldered with respect to the pad-surface at a 30° angle.

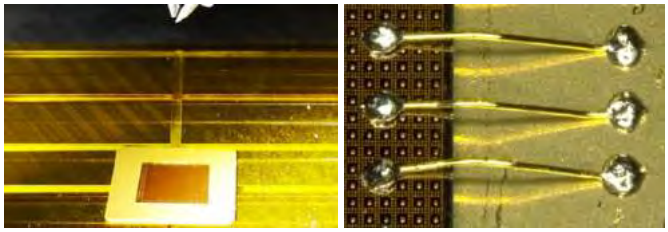

Figure 7: Test chip configuration with SB²-WB wire-bonds on "PacTech prototype system". Left image shows the bond situation. Right image shows the soldered wire-bonds.

The measured vertical strengths of the wire bond samples are presented in Figure 8.

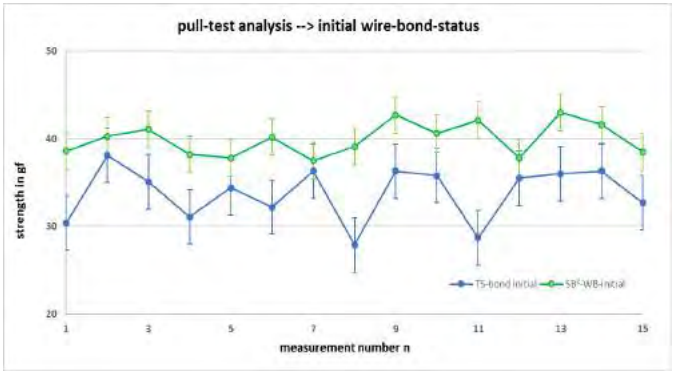

Figure 8: Pull test force measurement results of TS- and SB²-WB-bonds

The joint fractures were optically inspected and classified with a light microscope [17]. Figure 9 shows the resulting dominant fracture modes of the TS-bonds (left) and the SB²-WB-bonds (right) after pull test.

The average pull strengths for TS-bonds was found to be 33.8gf and 39.9gf for SB²-WB-bonds. While two different fracture modes were identified for the TS-bonds, SB²-WB-bonds always showed a wire-break phenomenon around the hook-location. The failure-modes associated with TS-bonds in the initial tests were diagnosed as neck-break (73%) and wire-break (27%) respectively.

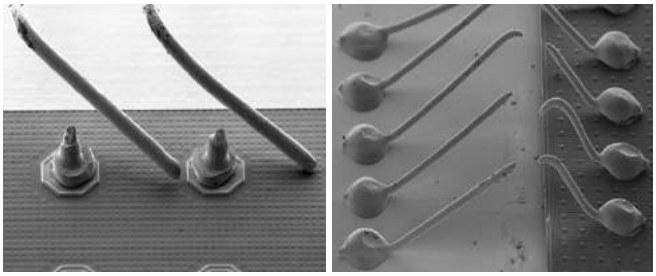

Figure 9: Dominant fracture modes after pull test. Left image shows neck-break fracture of TS-bonds. Right image shows fracture of SB²-WB-bonds.

A. Vibration test

In order to understand the mechanical performance and metallurgical stability of the soldered wire-bonds under stress, an initial vibration test was conducted which shed light on potential failure fractures. A "CTS RMS vibration tester" equipped with sinusoidal load feature was used to apply stress on the samples in x, y and z directions at a frequency range of 50-200Hz and an axis load of 5g for a time period of 8min.

The failure-mode distribution of the TS-bonds changed slightly to 50% neck-break and 50% wire-break and remained in 100% wire-break regime for the SB²-WB-bonds (Diagram 12). In both cases, the pull strength reduced (4.35% for TS- & 8.23% for SB²-WB-bonds), as illustrated in Diagram 13 that summarizes all measurement results.

In order to confirm that only the wires were weakening during the stress test and not the interface, additional shear tests on the SB²-WB-bonds were performed. The shear force measurement results before and after loading are presented in Figure 10.

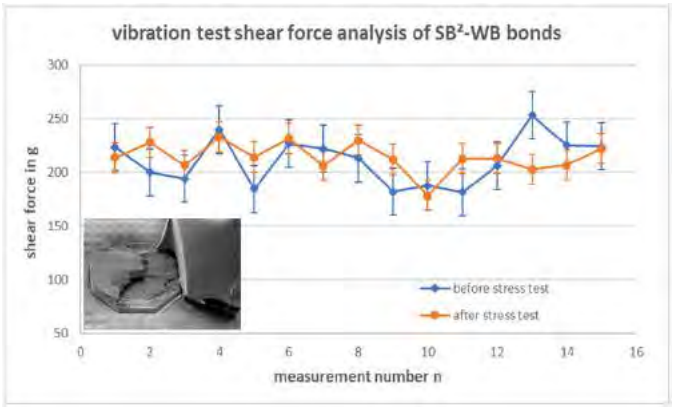

Figure 10: Shear force measurement results of SB²-WB-bonds before and after 3D vibration test

Moreover, the metallurgical properties at the interfaces of SB²-WB-bonds were analysed and inspected for fractures. The cross-sectional view of the interconnections before (left) and after tests (right) is shown in Figure 11.

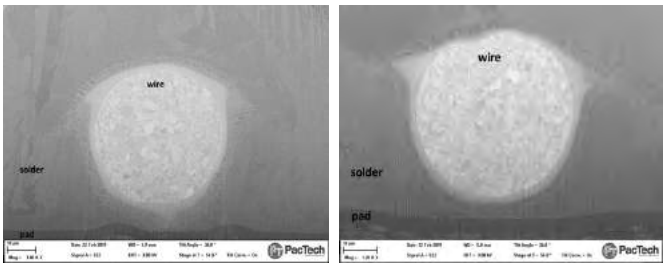

Figure 11: Cross-sectional views of SB²-WB-bonds before and after vibration test captured using SEM-FIB

For the examined range and configuration, the results show that both connections primarily lost the mechanical integrity in the bulk wire and not at the interface. Both bond-technologies withstood the massive mechanical load. Discrepancies in pull-tests results in the case of a wire breakage fracture mode have caused due to slight geometrical variances in the wire-bond build-up.

B. Climate test

The increased degradation of a soldered interface in comparison to a welded one is a widely recognized fact. To analyse and understand the degradation mechanism of the selected laser soldered wire-bond configuration in comparison to the TS-bonds, a temperature-cycle test in a 3-zone oven ("Vötsch VT 7012 S3") was performed. The temperatures ranged from -40°C in the cold-chamber to +125°C in the hot-chamber. The samples underwent 250 thermal cycles with a hold time of 30min in each chamber.

The failure-mode distribution of the TS-bonds indicated 60% neck-break, 37% wire-break and 3% ball-bond failure, as shown in figure 12. The inspection results of the SB²-WB bonds after pull test showed 90% wire-break and 10% wedge-metal-lift fracture-modes (Figure 12). The measurement results of the pull test are illustrated in Figure 13.

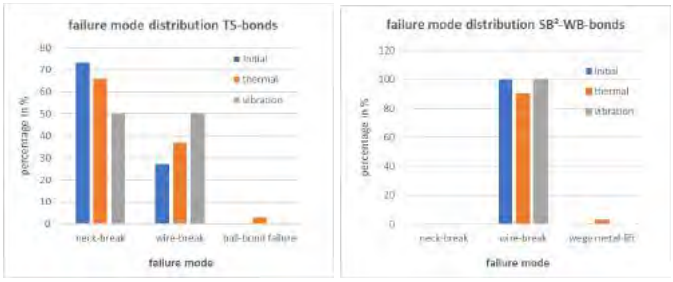

Figure 12: Distribution of fracture modes

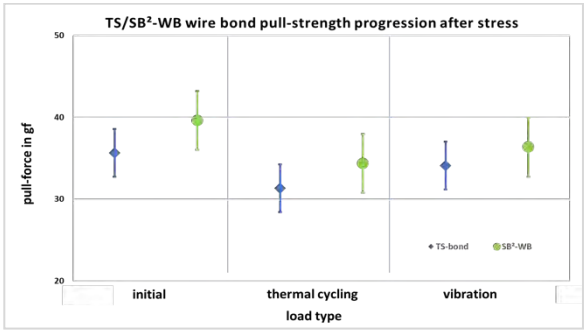

Figure 13: Pull strength measurement results

A reduction of the pull strength for TS-bonds of 12.7% and 13.2% for SB²-WB bonds was measured. Also in this case the fracture-modes of both connections primarily lose the mechanical integrity in the bulk wire and not at the interface.

Cross-sectional views of the laser soldered wire-bond interconnections after thermo-cycling tests are shown in Figure 14.

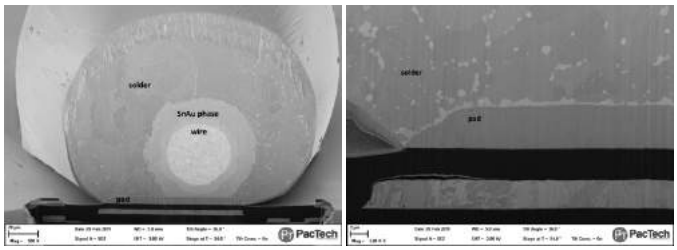

Figure 14: Cross-sectional views of SB²-WB-bonds after thermal cycling captured using SEM-FIB

After a period of 250 thermal cycles, an increase of the IMC-layer formation and an elongation of the SnAu diffusion zone were obvious, as expected. Neither cracks nor "Kirkendahl" voids were identified. The SnAu diffusion zone expanded by a factor of 4 and formed a stable and rotation symmetrical corona around the wire. The gradient of this micro structure shows a decreasing portion of Au towards the solder. The new SnAu material composition in this zone has a higher melting point than the basic solder material which might prevent further propagation of Au into the Sn.

During cross-sectional analysis of the TS-bond material structure no significant changes were identified after thermal cycling.

C. Ampacity test

Aside from evaluating mechanical and thermal performances, it is important to understand the electrical reliability especially for gaining insight into the process of laser-diode wire assembly on fragile GaAs devices where high load-currents are required. In contrast to TS-bonds, the solder-interface between wire and contact-pad presents an additional transition resistance. In the initial test, the wires were loaded with a ramp-up current until a break-down occurred in order to examine the dominant position of failure. To identify the weakest point, the tests were conducted and analysed with an infrared thermal imaging camera.

For this evaluation, two Au-coated "Kovar"-substrates were conjoined together with an epoxy insulating compound. A shift in the position generates a step in the package for the wire-bonds. On each of these test packages, four wires were bonded to connect both "Kovar"-elements for the voltage application. A black resist was applied on the wires to support thermal imaging. The test-setup is shown in Figure 15.

Figure 15: Test-setup for ampacity test sequence

The current was increased step-wise and applied for 0.2s. The waiting time between the cycles was 7s and each current cycle was repeated once. As evident in Figure 16, wire breakage event occurs with the TS-bonds and SB²-WB-bonds at 15A and 20A respectively.

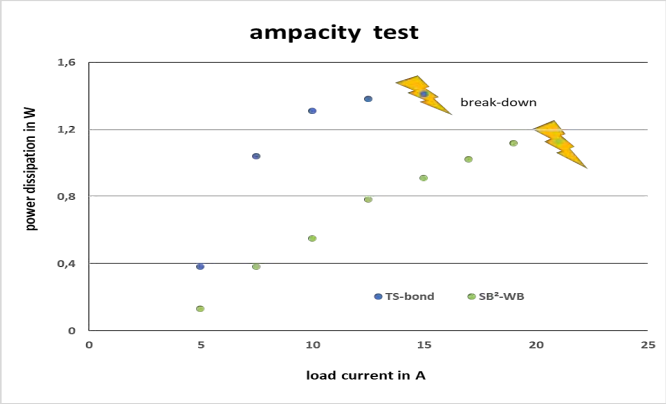

Figure 16: Current damage threshold measurement results

Representative thermal images during the test sequence for the TS-bonds (left) and for the soldered wire-bonds (right) are shown in Figure 17.

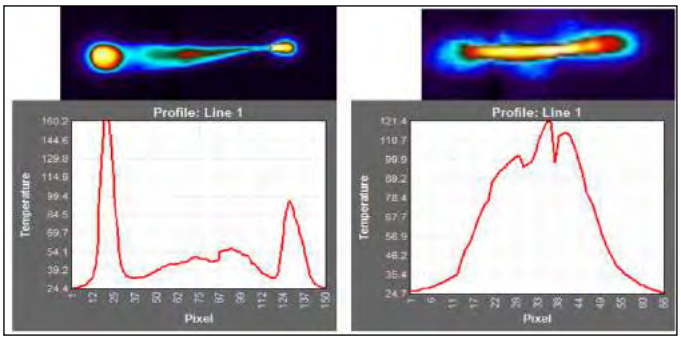

Figure 16. Thermal maps and corresponding temperature distribution of TS-bonds (left) and SB²-WB-bonds (right)

Each break-down occurred at the epicentre of the bent wire loop (Figure 18). The solder did not melt and lose contact at the wire interface as anticipated. Higher thermal mass of the selected solder volume, and consequently, larger available surface area for emitting thermal radiation prevented the incident of solder melting and component separation to occur. The thermal images show a more homogenous distribution of the heat in SB²-WB-bonds in contrast to the TS-bonds where distinct thermal peaks resemble the two different conjoined areas.

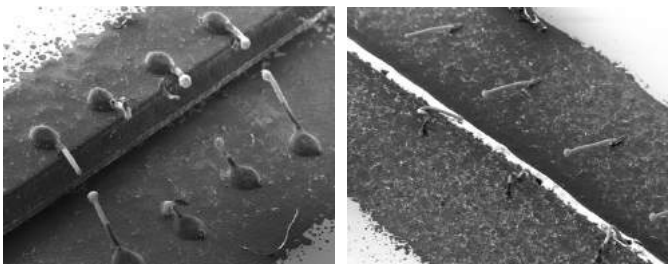

Figure 18: SEM pictures of wire-break fractures after electrical load. The left image shows SB²-WB-bonds and the right image shows TS-Bonds

Slight geometrical variances in the wire-bond build-up between TS and SB²-WB schemes is attributable to difference in specific resistances. This difference could be the underlaying root-cause for the differences in maximum load currents. Nevertheless, for the examined test range and configuration, the SB²-WB-bond configuration shows an enhanced electrical performance based on thermal distribution data.

IV. Application Prototype PDC-Sensor

A. *Process description*

This application deals with the laser-wire-soldering of piezoelectric actuator, which is the most important part of a PDC ultrasonic sensor. The underlying principle is to connect the piezoelectric actuator located at the bottom of an alumina chassis with two contact pins of the electrical connector interface. This construct is schematically depicted in Figure 19.

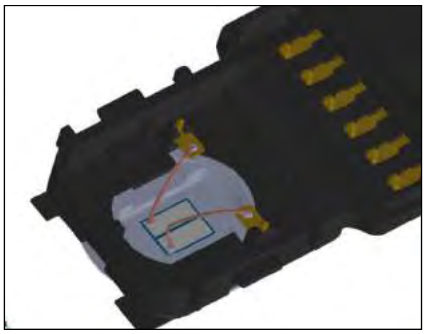

Figure 19: Model of bonded PDC-sensor package

The free work space available for bonding is 7.5mm x 10.68mm area with an orthogonal distance of 18mm between the pins and sensor surface. A wire length of 26mm with a diameter of 80µm is required to realize a reliable electrical contact with sufficient space for compensation of vibration. The wire material consists of Cu (2N) covered with a protective polyurethane resist coating. The contact-pad surface metallization of the PZT-piezo sensor element is electro-plated with a Ag-layer. The Cu contact pins are galvanically pre-tinned. In order to bond the Cu wire against the contact surfaces, SAC_305 solder with a spherical pre-form volume of 0.23mm³ is used.

This application is highly challenging and common wire-bonding technologies tend to fail due to either substrate breakage or insufficient bonding-strength [18].

B. *Process realization*

Particularly challenging steps involved the preparation of the bond-tool unit to contact the deep-seated sensor surface and removal of the polyurethane insulation coating around the wire during the bonding process. In order to prevent defects such as voids in the final bulk material caused by rapid evaporation of organic residues, the resist layer needs to be removed completely. This was realized using a precise pre-pulse with the built-in NIR laser-system. A sufficient thermal induced shrinkage was observed at a power density of 31J/m².

The first bond was formed on the sensor surface at an orthogonal wire direction with respect to the pin. The wire was

then positioned on the pin. This was followed by bonding with the solder sphere and severing of the wire. The bonding was realized with a NIR laser-pulse energy of 1400mJ (140W/10ms). Figure 5 shows the thermal plot of the optimized process-window.

C. *Analysis of process results*

In order to evaluate the interconnection quality, the generated wire-bonds were analysed with X-ray and SEM-FIB. With X-ray, bulk solder was scanned for any parasitic air inclusions, cracks and inhomogeneities. Figure 20 presents the X-ray measurement results.

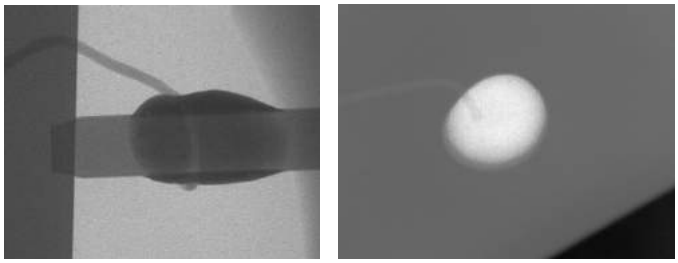

Figure 20: X-ray analysis of realized wire-bond interconnections. Left image shows bonded pin and right image shows the sensor surface bond

Both the bond-connections showed absence of any fractures or voids. The wire was stable and reliable surrounded by the 0.23mm³ solder volume. Metallurgical analysis of the solder wire interconnect using SEM-FIB is presented in Figure 21.

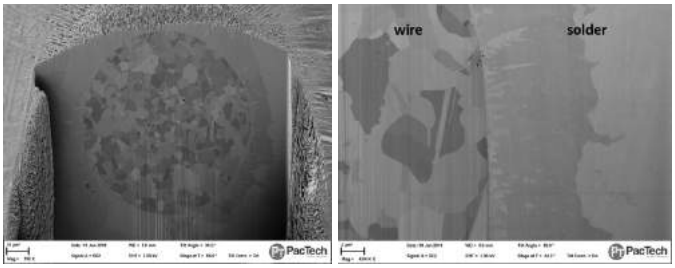

Figure 21.: SEM-FIB cross-section of Cu-SAC305 wire-bond interconnect

The cross-sectional view confirms a defect-free, high fidelity situation of the local interface. The IMC around the wire shows the preferred acicular metallurgic structure with a forming length of ca. 2-4µm.

An average resulting pull strength of 97.32gf in combination with solely wire-break fracture modes around the measurement hook-location confirms a mechanically stable wire joint structure.

V. Summary & Future prospect

- For the examined qualification range, the results discussed herein show that solder-wire-bond connections are reliable and deliver similar performance compared to conventional wire-bond technologies.
- The SB²-WB wire-bond is a versatile configuration with regard to solder volume and alloy type and allows the determination of the fracture position based on design.
- A soldered interconnection in contrast to conventional wire bonding can cover the whole surface of a pad, thus providing benefits from mechanical and thermal standpoints, especially on rectangular pad designs.
- The initial test sequences outlined herein along with the results from mechanical, electrical and thermal characterisation reflects only few aspects of a more complex wire-bonding technology and require additional evaluation and studies.
- The wire-bond soldering process creates homogenous and stable halo formations through diffusion processes around the embedded wire. The SAC_305/Au system outlined in the current work needs additional examination to a) verify whether further propagation of the Au into the Sn occurs, b) to evaluate the point of saturation and c) to consider other material compositions like Au80Sn20.
- Slight variations in the wire-bond built-up explain the discrepancies in pull tests results in case of identical fracture modes.
- In order to reach the stability level of a welded interface, high-melting solder alloys (HTS) can enable the transition from soldering to brazing [19].
- The generation of a stable and reliable Cu wire solder connection for Ag plated LTCC substrates is possible using SB²-WB wire-bond technology.

Future work involves detailed analysis of the soldered wire-bond connections along with specification of optimum process capabilities. Applications pertaining to bonding of wire bundles, ribbons and optical fibres will be explored. Wires corresponding to a wide range of diameters (15µm-600µm) will be investigated. The roadmap of SB²-WB process technology is illustrated in Figure 22.

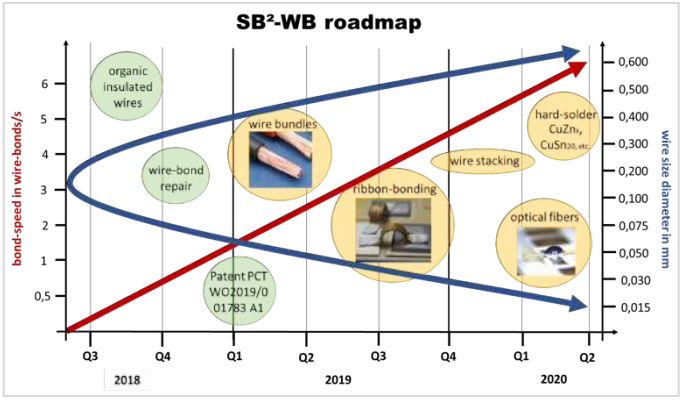

Figure 22.: SB²-WB process technology roadmap

VI. Appendixes

A. *Abbreviations and Acronyms*

SB² → Solder Ball Bumping

SB²-WB → Solder Ball Wire Bonding

TS → Thermosonic

PDC	→ Park Distance Control
PZT	→ Plumb Zirconate Titanate
LTCC	→ Low Temperature Co-fired Ceramic
MCM-D	→ Multi-Chip Module-Depositioned
EFO	→ Electronic Flame-Off
HAZ	→ Heat Affected Zone
ULL	→ Ultra Low Loop
SSB	→ Stand-Off-Stitch Bonds
HTS	→ High Temperature Solder
FHG-ENAS	→ Fraunhofer Institute for Electronic Nanos Systems

B. List of references

[1] TechSearch International, "Advanced Packaging Growth", 2017

[2] J.Phan, P.Fraud, "wire-bonding challenges in optoelectronic packagings", 1st SME Annual Manufacturing Technology Summit Deabron, 2004

[3] P.Kasulke, W.Schmidt, T.Oppert, „Solder Ball Bumper SB²-A flexible Manufacturing Tool for 3-dimensional Sensor and Microsystem Packages", 22th Inter. Electronics Manufacturing Technology Symposium, 1998

[4] User manual Optris CT

[5] Lee Levine, ASM International, "wire-bonding", EDFAAO, 2016

[6] ASIC Labor Heidelberg, "wire-bonding interconnections", workshop on Silicon Detectors, 2007

[7] Prof Dr. Salwani Mohd Daud, "IC Assembly, packaging and testing", DDE3253 Microelectronics

[8] Daniel Lu, C.P. Wong, "Materials for advanced packaging", Springer, 2009

[9] Lee R. Levine, "wire-bonding in optoelectronics", Advancing Microelectronic, 2002

[10] C.K.Charles Jr, K.J. Mach, R.L Edwards, "wire-bonding: Reinventing the process for MCM´s"

[11] U.Geißler, M.Schneider, "wire-bonding as dynamic process of hardening and softening", FHG-IZM

[12] Hiroshi Nishikawaa, Noriya Iwatab, "Formation and growth of intermetallic compound layers at the interface during laser soldering using Sn–Ag Cu solder on a Cu Pad", Journal of material processing technology, 2014

[13] W.Liu, C.Wang, M.Lie et al, "Comparison of AuSnx IMCs's Morphology", Distribution in Lead-free Solder Joints Fabricated by Laser and Hot Air Reflow Process", 6th Electronic Packaging Technology Conference, 2005

[14] H.Xu, C.Liu, V.Silberschmidt et al., "A micromechanism study of thermosonic gold wire-bonding on aluminium pad", Journal of Applied Physisc 108, 2010

[15] B.Chlyk, L.Levine, S.Babinetz et al., "Advanced Ultra-Low-Loop Wire Bonds", Semicon China, 2006

[16] Beng Teck Ng, Ganesh VP, Charles Lee, "Optimization of Gold Wire Bonding on Electroless Nickel Immersion Gold for high temperature Applications", IEEE, 2006

[17] Nordson Dage, "Finaler-Entwurf-Prüfdokument", 2016

[18] F.Seigneur, Y.Fournier, Th. Maeder et.al., "Laser soldering of piezoelectric actuator with minimal thermal impact", 2014

[19] S.Stein, J.Dippert, S.Roth et al., "Laser drop on demand micro joining for high temperature wire-bonding allications-system technology and mechanical joint performance"